AGU100 ADVANCING EARTH AND SPACE SCIENCE

Geophysical Research Letters

RESEARCH LETTER
10.1029/2018GL080501

Key Points:
- Collisions represent first-order processes in cold pool dynamics
- Cold pools lose circular shape shortly after birth
- Cold pools appear in clusters

Supporting Information:
- Supporting Information S1

Correspondence to:
G. Torri,
gtorri@hawaii.edu

Citation:
Torri, G., & Kuang, Z. (2019). On cold pool collisions in tropical boundary layers. *Geophysical Research Letters*, *46*, 399–407. https://doi.org/10.1029/2018GL080501

Received 17 SEP 2018
Accepted 7 DEC 2018
Accepted article online 17 DEC 2018
Published online 5 JAN 2019

On Cold Pool Collisions in Tropical Boundary Layers

Giuseppe Torri[1] **and Zhiming Kuang**[2,3]

[1]Department of Atmospheric Sciences, University of Hawai'i at Mānoa, Honolulu, HI, USA, [2]Department of Earth and Planetary Sciences, Harvard University, Cambridge, MA, USA, [3]John A. Paulson School of Engineering and Applied Sciences, Harvard University, Cambridge, MA, USA

Abstract Collisions between cold pools are generally acknowledged to be important processes through which new convective cells are triggered. Yet relatively little has been done to characterize these processes in detail, quantify their impact on the life cycle of cold pools, and include them in convective parameterizations. We use a combination of Eulerian and Lagrangian models to investigate how much cold pools are affected by collisions. Results from simulations in radiative-convective equilibrium suggest that collisions represent a first-order process in the dynamics of cold pools, the median time of first collision being under 10 min since cold pool birth. Through a Lagrangian tracking algorithm, it is also shown that cold pools are significantly deformed by collisions and lose the circular shapes they would have if in isolation only a few minutes after birth. Finally, it is suggested that cold pools happen in clusters, and associated spatial and temporal scales are presented.

Plain Language Summary While collisions between cold pools are known to be key processes in the formation of new convective clouds, they are overlooked by many studies and most parameterizations. We find that collisions have a significant impact on the life and the dynamics of cold pools, affecting their propagations in the boundary layer already few minutes after their birth. Contrary to many conceptual models, our results suggest that cold pools lose circular symmetry already when still young. Finally, we show that cold pools are not randomly distributed in space and time but tend to appear in clusters.

1. Introduction

Cold pool collisions represent a key process in the generation of deep convective elements. Purdom (1976) and Weaver and Nelson (1982) were among the first to argue that the areas where cold pools collide coincide with the areas where new convective cells are generated. This was later confirmed by Droegemeier and Wilhelmson (1985a, 1985b), who showed that, as cold pools collide, the positive pressure anomalies in their heads can help generate vertical pressure gradients that can accelerate parcels to their level of free convection (Houze, 1994). This picture has been corroborated by many studies (see e.g., Feng et al., 2015; Jeevanjee & Romps, 2015; Khairoutdinov & Randall, 2006; Lima & Wilson, 2008; Moncrieff & Liu, 1999; Moseley et al., 2016; Rio et al., 2009; Rotunno et al., 1988; Skamarock et al., 1994; Torri et al., 2015; Weisman & Rotunno, 2004; Wilson & Schreiber, 1986).

For a number of years, it was believed that collisions played a lesser role in convective systems with low wind shear over the tropical ocean, given that such cold pools tend to be weaker and shallower than their mid-latitude continental counterpart. Tompkins (2001) suggested that, in the former cases, convective cells are triggered by a thermodynamic effect, whereby the moisture anomalies often observed around the edges of cold pools lower the convective inhibition experienced by air parcels originating from those areas. This idea was tested in recent years (Torri et al., 2015) and, while thermodynamic effects were still found to be important, results indicated that convection triggering in a case similar to the one examined by Tompkins (2001) still requires the action of gust fronts to lift parcels from the surface.

Collisions of cold pools, or, more precisely, of gravity currents, have also been studied in other contexts. For example, Simpson (1997) examined the collision of two gravity currents in a tank of water, showing the creation of two bores traveling in opposite directions following the collision. Along with theoretical work to predict the propagation speed of the bores resulting from the collision, Shin (2001) also presented results of experiments on colliding gravity currents of different heights but equal densities. This work was recently

extended by van der Wiel et al. (2017) who, in order to better understand the collision between sea breeze fronts, investigated the effects of height as well as initial density differences between gravity currents colliding in a water tank. More recently still, collisions were at the center of two studies: Cafaro and Rooney (2018) considered the behavior of the interfacial slope of two colliding currents with an idealized numerical and a theoretical approach, whereas Zhong et al. (2018) conducted lock-exchange experiments with equal gravity currents to quantify the turbulent mixing at the time of collision.

Colliding gravity currents, whether sea breezes, downslope katabatic flows, or cold pools, are a common occurrence in nature. Yet so many aspects regarding this phenomenon remain to be understood. In the context of deep convection over a tropical ocean, we are interested in quantifying the importance of collisions in the overall cold pool dynamics. In the following, we will present evidence supporting the idea that not only are collisions important, but they represent a first-order process in the life cycle of a cold pool, and, therefore, should not be neglected in any simple cold pool model.

2. Methods

In our work, we used a numerical model known as System for Atmospheric Modeling (SAM), version 6.8.2, which solves the anelastic equations of motion and uses liquid water static energy and nonprecipitating and precipitating total water as thermodynamic prognostic variables (Khairoutdinov & Randall, 2003). Doubly periodic boundary conditions were imposed in the horizontal directions, and a sponge layer was placed in the upper-third of the domain to absorb reflected gravity waves. Using SAM, we conducted a total of 13 simulations, each initialized using random noise with different seeds, over an oceanic surface with a temperature held fixed at 302.65 K. Each simulation was first spun up for 30 days until radiative-convective equilibrium (RCE) was reached, and then restarted for 12 hr. One of the simulations was run along with the Lagrangian Particle Dispersion Model (see e.g., Nie & Kuang, 2012; Torri et al., 2015; Torri & Kuang, 2016a, 2016b). Details of the setup for the simulations conducted with SAM and the Lagrangian Particle Dispersion Model are given in the supporting information (Blossey et al., 2010; Collins et al., 2006; Lin et al., 1983; Nie & Kuang, 2012; Torri et al., 2015; Torri & Kuang, 2016a, 2016b).

In order to illustrate the impact of cold pools on the distances between clouds, we want to compare the RCE simulations with a case that, while featuring a number of convective clouds, does not have cold pools. Inhibiting rain evaporation in the subcloud layer could seem like a straightforward approach to hinder the formation of cold pools (see e.g., Boing et al., 2012; Jeevanjee & Romps, 2013; Khairoutdinov & Randall, 2006). However, in such cases, moist convection aggregates relatively quickly, and the presence of convective clouds is limited to a single patch in the domain. Therefore, we decided to carry out the comparison using a case of shallow convection instead. We ran an additional simulation initializing the model with soundings, surface fluxes, and large-scale forcing taken from the undisturbed phase of the Barbados Oceanographic and Meteorological Experiment (BOMEX; see e.g., Siebesma et al., 2003). We refer the reader to the supporting information for further details regarding the setup used for this case.

A concept we will frequently use is that of *cloud center*. For the RCE case, we begin by selecting an altitude of 2,594 m in the model domain. Selecting a precise altitude leaves us with a $(2 + 1)$-dimensional space, which we will refer to as $\mathbb{S}$, spanned by the time and the horizontal dimensions. In this space, we select points that are contiguous with respect to a 6-point 3-D connectivity, and for which the precipitating water mass mixing ratio, q_p, is above 1.0 g/kg. If the resulting cluster contains more than 500 points, we compute the average of the positions of all the selected grid points, taking the periodicity of the horizontal directions into account, and define that as the center of a cloud. We have tested the sensitivity of our results to using a 26-point 3-D connectivity, varying by 50% the threshold of q_p, or by changing the number of points used to define a cloud center, and found our results to be relatively insensitive to these changes.

Finally, the definition of cloud center is similar in the BOMEX case, except that we used an altitude of 2,500 m and the condition of nonprecipitating water mass mixing ratio, q_n, to be higher than 0.1 g/kg is used in order to identify a cloud center. The choice of using this particular variable instead of q_p was due to the fact that clouds in our BOMEX experiment do not precipitate. Notice that, for consistency, we could have used q_n as a variable in the analysis of the RCE case as well. However, because we want to make sure that the clouds selected in that case do actually generate cold pools, using precipitating water seemed like a better choice.

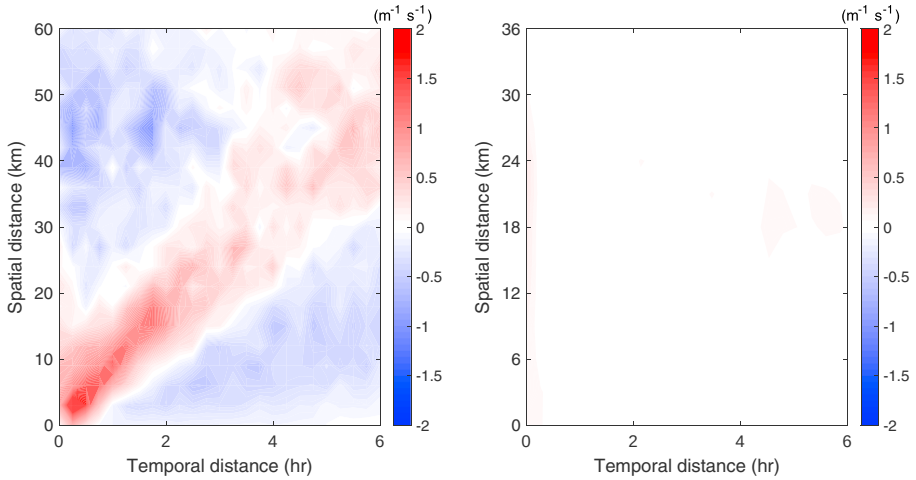

Figure 1. (left) Difference between the histograms of spatial and temporal distances between cloud centers in the ensemble of simulations considered in this study and an ensemble of randomly distributed cloud centers. (right) Same as left, but for the Barbados Oceanographic and Meteorological Experiment case.

3. Results

We start by considering the web of distances between all cold pools. We will assume that every cold pool has been generated by a deep convective cloud, which means we can focus on distances between clouds (cf. Text S2). This can be done using the concept of cloud centers introduced in the previous section. Because we will not assume any velocity scale that will allow us to compare time and space directions, we will compute spatial and temporal distances separately. Once we have determined the distances between every pair of cloud centers, we build a bivariate histogram, which we will refer to as the *control histogram*. Then, we consider the same number of cloud centers, but we distribute them randomly in space and time, and we compute the histogram for this configuration; we do this for a total of 10 random configurations and refer to the resulting average as the *random histogram*. This procedure is repeated for the other 12 simulations conducted using SAM. Finally, we compute the difference between the ensemble-averaged control histograms and the random histograms, where each histogram has been normalized by the number of pairs of cloud centers, $N(N+1)/2$, N being the total number of cloud center in each simulation, and show the result in the left panel of Figure 1 (see Figure S3 for a normalized version).

The oblique red band suggests that clouds are related through a phenomenon that propagates at a given speed. Considering each time slice in Figure 1, we can select the distance where the maximum value occurs and use this to determine the propagation speed associated with the red band. Averaging together the results for the first 3 hr of propagation, where the band seems to be most coherent, we find an average value of 1.78 m/s. Except at high vertical modes, gravity waves tend to have much higher propagation speeds (Mapes, 1993), which would make cold pools a more reasonable candidate to explain the presence of the red band. Assuming these could be approximated as gravity currents, their expected propagation speed would be related to their thermodynamic properties by (see e.g., Cotton et al., 2011)

$$c = Fr\left(gh\frac{\Delta\theta_\rho}{\overline{\theta_\rho}}\right)^{1/2}, \tag{1}$$

where Fr is the Froude number, g is the gravitational acceleration, h is the height of the gravity current, and $\overline{\theta_\rho}$ is the average density potential temperature. Using a Froude number equal to 1 for simplicity (Wakimoto, 1982), a cold pool height of 250 m (Torri & Kuang, 2016b), and $\overline{\theta_\rho}$ equal to 300 K, we obtain a $\Delta\theta_\rho$ associated with the cold pool of 0.4 K, which appears to be of the same magnitude as the cold pools we observe in our simulations (see Figure S2 for an illustrative example). Notice that the temporal distance between two cloud centers also includes the time required for a triggered updraft to grow and generate sufficient precipitation to satisfy the criteria for the identification of cloud center. This would suggest we are underestimating the $\Delta\theta_\rho$ of cold pools associated with the red band.

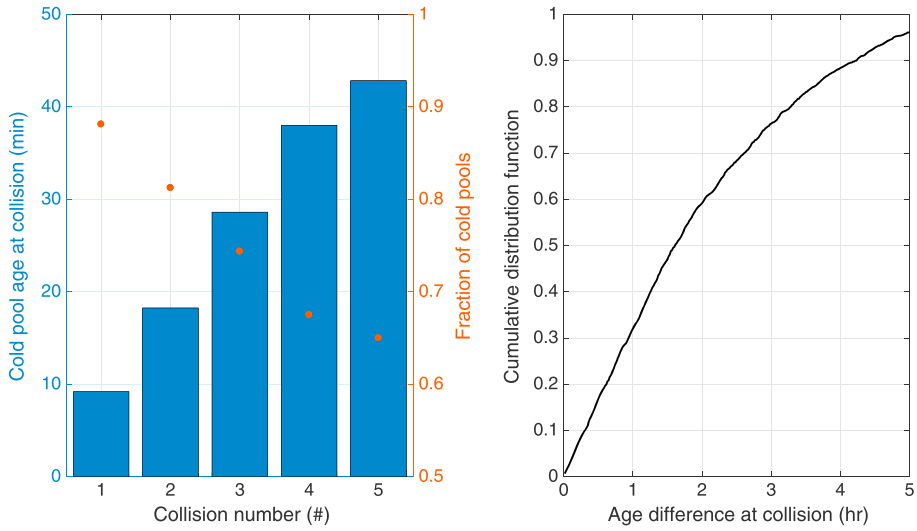

Figure 2. (left) Each blue bar represents the median time of collision for a given collision number, while the orange dots indicate the fraction of cold pools that have undergone as many collisions. (right) Cumulative distribution function of differences between the age of a given cold pool and that of another cold pool colliding with it.

One surprising feature looking at Figure 1 is that the band extends almost completely to the origin of the space-time graph, suggesting that many clouds or, equivalently, cold pools are very close in space and in time. In turn, this would imply that, in many cases, cold pools are impacted by collisions shortly after their birth.

In order to verify whether the red band observed in the left panel of Figure 1 is really due to cold pools, we repeated the calculation of the histogram using the BOMEX run instead, the results being shown in the right panel of the figure. The plot does not differ significantly from zero anywhere, thus reinforcing our interpretation of the results obtained for the RCE case. Notice also that, in spite of what visual inspection of the model outputs might suggest, Figure 1 indicates that the position of convective clouds could be thought of as random only in the nonprecipitating case simulated in this study (the recent work by Bretherton & Blossey, 2017, suggests care should be taken before generalizing to all shallow cumulus cases). In the RCE cases shown above, cold pools break the symmetry.

Next, we turn our attention to the cold pool tracking algorithm, we focus on the lowest model level, and save the positions of every cold pool grid box for all model times. Using some geometrical intuition, it is clear that the bottom level and the time dimension span a three-dimensional space in which cold pools appear as clusters. We then examine every grid box of each cold pool in this space, and, if its neighborhood—in the sense of 6-point 3-D connectivity in the $(2+1)$-dimensional space we are considering—contains the grid box of a different cold pool, we mark it as a *collision box*. We say two cold pools have collided when they share more than 40 collisions boxes. Since the search for neighboring cells takes place in a space that includes the temporal dimension, the 40 collision boxes are to be intended as accumulated in time. There is no special alchemy that led us to choose this particular threshold: it was simply to ensure collisions are significant. We have verified that our conclusions are robust to the value chosen.

We record how many collisions each cold pool experiences and at what point in the life of a cold pool each happens. The blue bars in the left panel of Figure 2 represent the median values of the times of the first five collisions experienced by cold pools. Because not all cold pools undergo five collisions in their life cycle, we use the orange dots to mark the fraction of total cold pools that contribute to the calculation for a given collision number. The position of the first dot does not necessarily imply that 11.9% of cold pools never experience collisions, but simply that that fraction never has a collision made of 40 collision boxes. Although a change in this threshold does not lead to qualitative changes of our results, small quantitative changes can still happen. This figure essentially confirms how collisions between cold pools tend to happen even at very early stages of their evolution: the median value of the first collision is little less than 10 min, and the median of the fifth collision is 42.8 min.

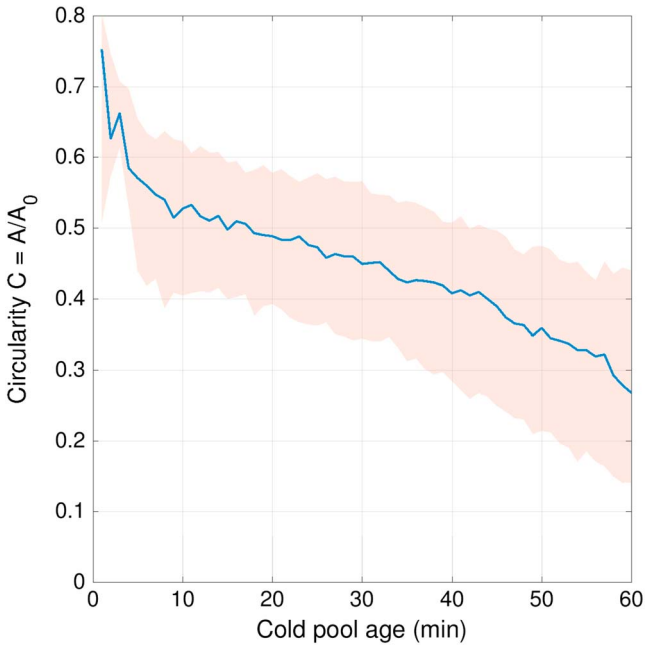

Figure 3. Median of the distribution of the circularity C as a function of cold pool age. The red band is bounded below by the 5th percentile of the distribution and above by the 95th percentile.

There is the possibility that most collisions take place between a relatively young cold pool and an extremely old one (Tompkins, 2001). In this case, the gust front of the older cold pool would likely be extremely weak, and therefore this collision would be a mere contact with no great repercussions on the expansion of the younger cold pool. To check whether this is the case, we also determine the age difference between cold pools at the time of their collision, and show its cumulative distribution in the right panel of Figure 2. Although there does seem to be a longer tail toward large time differences, notice that 32.0% of cold pools have an age difference smaller than 60 min when colliding, and the median of the distribution is 97 min of age difference. This would suggest that the gust fronts of most colliding cold pools are still strong enough to impact the other cold pool.

We can further use the Lagrangian tracking algorithm to try and better quantify the impact of collisions by considering the temporal evolution of each cold pool's *circularity*, which we here define as $C = A/A_0$, where A is the area of the cold pool at the surface and A_0 that of the smallest circle enclosing it. Because isolated cold pools should have approximate cylindrical symmetry, the ratio between their area at the surface and that of the smallest circle containing them should be close to 1. If, on the other hand, collisions deform cold pools in their evolution, the ratio should be lower, the degree of the departure depending on the deformation. The blue line in Figure 3 represents the median value of the distribution of circularity as a function of cold pool age; the orange band is the area spanned by the evolution of the 5th and 95th percentiles of said distribution. Results show that the ratio starts off at values relatively close to 1 and then quickly decays over time, suggesting that collisions have a significant impact on the life cycle of cold pools even from early stages. The discretization of the horizontal space conducted using squares of finite size means circles of small radius are not well represented. In turn, this implies that circularity might be underestimated during the very initial stages of the cold pool propagation.

Given that collisions appear to be an important process in cold pool dynamics and that cold pools tend to be quite young when colliding, it is natural to wonder whether collisions happen randomly everywhere or if they tend to be localized, and, if so, whether we can associate scales to the clustering. In order to investigate this point, we recall the definition of Boltzmann entropy (Huang, 1987). Let us consider a gas of N identical particles, and let us assume that they can be divided in subgroups of N_i particles. Particles within each subgroup are in a similar microscopic state, called *microstate*. Because the particles are identical, those having the same microstate can be exchanged without altering the state of the gas, referred to as *macrostate*. The Boltzmann entropy for the system can be defined as

$$S(\sigma, \tau) = k_B \ln(\Omega), \tag{2}$$

where Ω is the number of microstates that yields the same observed macrostate and k_B is the Boltzmann constant. Let us now suppose that the N identical particles are the cloud centers previously introduced, and let us partition the space $\mathbb{S}$ into $m_{\sigma,\tau}$ boxes that measure σ in each horizontal direction and τ in the temporal direction. Each box can be considered as a microstate of the system, and the collection of numbers of cloud centers, $(N_1, N_2, \ldots, N_{m_{\sigma,\tau}})$, as a macrostate. The number of microstates for a given macrostate is given by

$$\Omega(\sigma, \tau) = \frac{N!}{\prod_{i=1}^{m_{\sigma,\tau}} N_i!}. \tag{3}$$

Let us now consider two cases with uniform distributions of N cloud centers: in the first case, the support of the distribution is the entire $\mathbb{S}$; in the other case, the distribution is still uniform, but its support is limited to a subspace. If we partition $\mathbb{S}$ into $m_{\sigma,\tau}$ boxes, each box will contain $N/m_{\sigma,\tau}$ cloud centers in the first case and $N/m'_{\sigma,\tau}$ in the second, where $m'_{\sigma,\tau}$ is some integer smaller than $m_{\sigma,\tau}$. We will denote the entropies computed

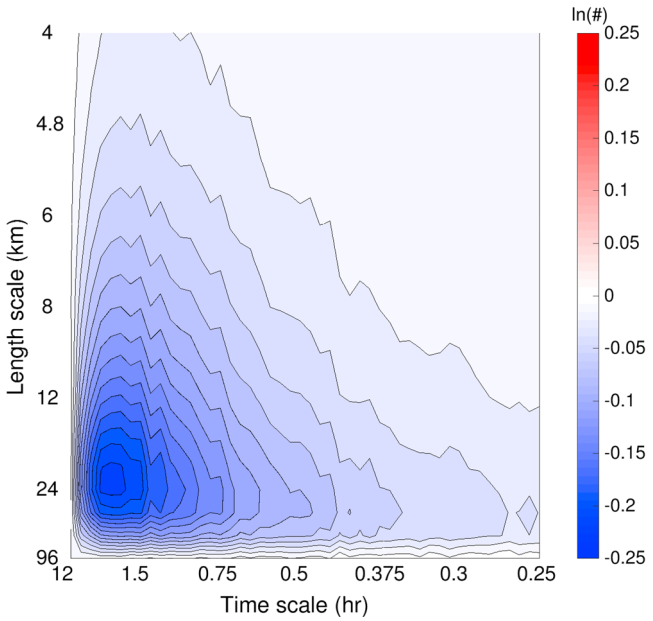

Figure 4. Difference of entropies, $S'(\sigma,\tau) - S(\sigma,\tau)$, averaged over the ensemble of System for Atmospheric Modeling simulations considered and normalized by the Boltzmann constant and by the number of cloud centers in each simulation. The axes indicate the number of boxes a dimension is partitioned into, or, equivalently, the corresponding size of each box. Solid contours are every 0.015 units.

in the two cases as $S(\sigma,\tau)$ and $S'(\sigma,\tau)$, respectively. Assuming that $N/m_{\sigma,\tau} \gg 1$ and that $N/m'_{\sigma,\tau} \gg 1$, we can use the Stirling's approximation and show that

$$\frac{S'(\sigma,\tau) - S(\sigma,\tau)}{k_B} = -m'_{\sigma,\tau} \ln\left[\left(\frac{N}{m'_{\sigma,\tau}}\right)!\right] + m_{\sigma,\tau} \ln\left[\left(\frac{N}{m_{\sigma,\tau}}\right)!\right] \sim -N \ln\left(\frac{m_{\sigma,\tau}}{m'_{\sigma,\tau}}\right). \tag{4}$$

Equation (4) seems to suggest that, for a given partition, the difference between the two entropies is greatest in magnitude when $m_{\sigma,\tau}$ is the greatest and $m'_{\sigma,\tau}$ is the smallest. This means that the difference is extremized by a partition whose number of particle-containing boxes in the clustered case is the smallest. Because of this, the difference between the entropy of a cluster of points and that of a uniform distribution of the same number of points could be used to estimate the size of the cluster: given a distribution of cloud centers, compute the entropy $S'(\sigma,\tau)$ for all possible values of σ and τ, and compare it with the entropy $S(\sigma,\tau)$ of the same number of points uniformly distributed in $\mathbb{S}$; the point where the absolute value of this difference is maximized corresponds to the spatial and temporal scales of the clustering.

Because the spatial dimensions of $\mathbb{S}$ have periodic boundary conditions, there is an ambiguity in deciding the positions of the boxes that make up a partition: due to their equal sizes, their positions will be automatically decided once the first box is drawn, but this leaves a degree of freedom as to where to break the symmetry and place this first box. In order to rid of this problem, we can consider a large ensemble of discretizations, each with a different position of the boxes. For each SAM simulation, we compute the entropy associated with the diagnosed cloud centers, then that of the same number of points randomly distributed in time. This is repeated 500 times with boxes in different positions, as discussed above. The difference of the two quantities is averaged across the ensemble and shown in Figure 4. For convenience, we have normalized it by the Boltzmann constant. We have also normalized the entropy difference for each ensemble member by the number of cloud centers N in that ensemble. Equation (4) suggests that this is a better way to average quantities computed for cases having different cloud centers, while giving, at the same time, a more intuitive way to understand the difference between entropies: modulo a logarithm, this can essentially be thought of as related to the ratio between the space occupied the cloud centers in the control case and the entire space $\mathbb{S}$. From Figure 4, it appears that cold pools tend to cluster with a spatial scale of 24 km and a temporal scale of 2.4 hr.

One caveat we wish to point out is that the space $\mathbb{S}$ built from the numerical simulations conducted with SAM has a finite size and is essentially discretized, in time as well as in space. This implies that the sizes of the boxes we partition $\mathbb{S}$ with must divide the sizes of the larger domain. The repercussions of this are felt particularly at large spatial and temporal scales, which allows for a degree of uncertainty on the precise value that we interpret as a scale for the clustering of cold pools.

4. Discussion

The results presented in this work challenge some of the assumptions or common practices used when dealing with conceptual models of cold pools. For example, in their cold pool parameterization, Grandpeix and Lafore (2010) and Grandpeix et al. (2010) assumed that cold pools had a circular shape and that collisions were essentially coalescence processes. More recently, Romps and Jeevanjee (2016) proposed a simple model to predict the lifetime and the final size of cold pools, and Grant and van den Heever (2016) carefully examined the way in which surface heat fluxes affect cold pool dissipation rates, both studies considering the expansion of an isolated cold pool. In no way do our findings contradict or challenge the validity of the cited results, but they do pose some question on their applicability to a scenario with many cold pools, such as the one examined here in RCE: if cold pools collide with other cold pools soon after their formation, they might entrain air which is colder than the environment, and thus be able to live longer and reach a greater size than they would have, had they not collided; furthermore, if a cold pool collides with a younger cold pool, the former might override the latter, and not feel the effects of surface fluxes anymore.

Another interesting finding that deserves some comment is the existence of spatial and temporal clustering scales suggested by the difference in entropies presented in Figure 4. This is in contrast with the assumption of a uniform cold pool distribution of Grandpeix and Lafore (2010), but it is in good agreement with the observation of Feng et al. (2015), who reported that the deep convective clouds they observed did not appear randomly distributed, but rather in clusters having a size of tens of kilometers. The authors went further to suggest that, through this clustering, updrafts shield each other from entraining drier air from the environment, and can therefore grow to greater depths. Given their potential role in the shallow-to-deep transition, a deeper understanding of these scales, particularly the factors determining them, is a task of great importance that we shall undertake in future work.

5. Conclusions

The work presented in this manuscript has focused on providing a quantitative characterization of the importance of collisions in the life cycle of cold pools.

In section 3, the histogram of distances between all the cloud centers was determined, and the difference between this and the equivalent histogram constructed using an ensemble of equal numbers of fictitious cloud centers distributed randomly in space-time was presented. A relatively large number of points near the origin of the coordinate axes suggested that many cloud centers are very close both in space and in time.

Using a Lagrangian tracking algorithm, each cold pool was then considered, and every collision with other cold pools was recorded. Particular attention was given to the time at which each collision takes place relative to the time of birth of the examined cold pool and the difference of ages between said cold pool and the other one participating in the collision. Results showed that collisions happen rather quickly after the formation of a cold pool, the median of the distribution of first collision times being just under 10 min, and that cold pools that are colliding are also relatively young.

Next, the tracking algorithm was used to examine the shape of cold pools as they evolve in the boundary layer. At each time, the ratio between the area of the cold pool and that of the smallest circle containing it was examined. Findings from all the cold pools suggest that the median of this ratio tends to decay rather quickly in time, which, in turn, would imply cold pool shapes being significantly affected by the collisions. The collection of results obtained would suggest that collisions represent a first-order process in the life cycle of cold pools.

Finally, the question of whether cold pools are uniformly distributed or if they tend to appear in clusters was examined using the definition of Boltzmann entropy. Considering the distribution of points in each of the simulations as a macrostate, the three-dimensional space in which cloud centers are defined was divided in subgroups, each representing a microstate. Then, the entropy associated with this system was computed

and compared with the entropy of a system containing the same number of points randomly distributed in space-time. This difference was determined for a variety of box sizes, with the idea that it would be extremized at the clustering spatial and temporal scales, which were found to be 24 km and 2.4 hr, respectively.

Acknowledgments
The authors thank Susan van den Heever and Leah Grant for enlightening discussions and Paul Edmon and Plamen Krastev for assistance with the Harvard Odyssey cluster on which the simulations were run. This research was supported by the Office of Biological and Environmental Research of the U.S. DOE under grant DE-SC0018120 as part of the ASR Program and NSF grant AGS-1649819. The data for this paper are available at http://doi.org/10.5281/zenodo.1482006.

References

Boing, S. J., Jonker, H. J. J., Siebesma, A. P., & Grabowski, W. W. (2012). Influence of the subcloud layer on the development of a deep convective ensemble. *Journal of the Atmospheric Sciences*, *69*(9), 2682–2698. https://doi.org/10.1175/JAS-D-11-0317.1

Blossey, P. N., Kuang, Z., & Romps, D. M. (2010). Isotopic composition of water in the tropical tropopause layer in cloud-resolving simulations of an idealized tropical circulation. *Journal of Geophysical Research*, *115*, D24309. https://doi.org/10.1029/2010JD014554

Bretherton, C. S., & Blossey, P. N. (2017). Understanding mesoscale aggregation of shallow cumulus convection using large-eddy simulation. *Journal of Advances in Modeling Earth Systems*, *9*, 2798–2821. https://doi.org/10.1002/2017MS000981

Cafaro, C., & Rooney, G. G. (2018). Characteristics of colliding density currents: A numerical and theoretical study. *Quarterly Journal of the Royal Meteorological Society*, *144*(ja), 1761–1771. https://doi.org/10.1002/qj.3337

Collins, W. D., Rasch, P. J., Boville, B. A., Hack, J. J., McCaa, J. R., Williamson, D. L., et al. (2006). The formulation and atmospheric simulation of the Community Atmosphere Model version 3 (CAM3). *Journal of Climate*, *19*(11), 2144–2161. https://doi.org/10.1175/JCLI3760.1

Cotton, W. R., Bryan, G., & van den Heever, S. C. (2011). Chapter 8—Cumulonimbus clouds and severe convective storms. In W. R. Cotton, G. Bryan, & S. C. van den Heever (Eds.), *Storm and cloud dynamics: The dynamics of clouds and precipitating mesoscale systems, international geophysics* (Vol. 99, pp. 315–454). Cambridge, MA: Academic Press. https://doi.org/10.1016/S0074-6142(10)09914-6

Droegemeier, K. K., & Wilhelmson, R. B. (1985a). Three-dimensional numerical modeling of convection produced by interacting thunderstorm outflows. Part I: Control simulation and low-level moisture variations. *Journal of the Atmospheric Sciences*, *42*(22), 2381–2403. https://doi.org/10.1175/1520-0469(1985)042<2381:TDNMOC>2.0.CO;2

Droegemeier, K. K., & Wilhelmson, R. B. (1985b). Three-dimensional numerical modeling of convection produced by interacting thunderstorm outflows. Part II: Variations in vertical wind shear. *Journal of the Atmospheric Sciences*, *42*(22), 2404–2414. https://doi.org/10.1175/1520-0469(1985)042<2404:TDNMOC>2.0.CO;2

Feng, Z., Hagos, S., Rowe, A. K., Burleyson, C. D., Martini, M. N., & Szoeke, S. P. (2015). Mechanisms of convective cloud organization by cold pools over tropical warm ocean during the AMIE/DYNAMO field campaign. *Journal of Advances in Modeling Earth Systems*, *7*, 357–381. https://doi.org/10.1002/2014MS000384

Grandpeix, J.-Y., & Lafore, J.-P. (2010). A density current parameterization coupled with Emanuel's convection scheme. Part I: The models. *Journal of the Atmospheric Sciences*, *67*(4), 881–897. https://doi.org/10.1175/2009JAS3044.1

Grandpeix, J.-Y., Lafore, J.-P., & Cheruy, F. (2010). A density current parameterization coupled with Emanuel's convection scheme. Part II: 1D simulations. *Journal of the Atmospheric Sciences*, *67*(4), 898–922. https://doi.org/10.1175/2009JAS3045.1

Grant, L. D., & van den Heever, S. C. (2016). Cold pool dissipation. *Journal of Geophysical Research: Atmospheres*, *121*, 1138–1155. https://doi.org/10.1002/2015JD023813

Houze, R. A. J. (1994). *Cloud dynamics, International geophysics* (Vol. 53). Cambridge, MA: Academic Press.

Huang, K. (1987). *Statistical mechanics* (2nd ed.). John Wiley and Sons, Ltd.

Jeevanjee, N., & Romps, D. M. (2013). Convective self-aggregation, cold pools, and domain size. *Geophysical Research Letters*, *40*, 994–998. https://doi.org/10.1002/grl.50204

Jeevanjee, N., & Romps, D. M. (2015). Effective buoyancy, inertial pressure, and the mechanical generation of boundary layer mass flux by cold pools. *Journal of the Atmospheric Sciences*, *72*(8), 3199–3213. https://doi.org/10.1175/JAS-D-14-0349.1

Khairoutdinov, M. F., & Randall, D. A. (2003). Cloud resolving modeling of the ARM summer 1997 IOP: Model formulation, results, uncertainties, and sensitivities. *Journal of the Atmospheric Sciences*, *60*(4), 607–625. https://doi.org/10.1175/1520-0469(2003)060<0607:CRMOTA>2.0.CO;2

Khairoutdinov, M., & Randall, D. (2006). High-resolution simulation of shallow-to-deep convection transition over land. *Journal of the Atmospheric Sciences*, *63*(12), 3421–3436. https://doi.org/10.1175/JAS3810.1

Lima, M. A., & Wilson, J. W. (2008). Convective storm initiation in a moist tropical environment. *Monthly Weather Review*, *136*(6), 1847–1864. https://doi.org/10.1175/2007MWR2279.1

Lin, Y.-L., Farley, R. D., & Orville, H. D. (1983). Bulk parameterization of the snow field in a cloud model. *Journal of Climate and Applied Meteorology*, *22*(6), 1065–1092. https://doi.org/10.1175/1520-0450(1983)022<1065:BPOTSF>2.0.CO;2

Mapes, B. E. (1993). Gregarious tropical convection. *Journal of the Atmospheric Sciences*, *50*(13), 2026–2037. https://doi.org/10.1175/1520-0469(1993)050<2026:GTC>2.0.CO;2

Moncrieff, M. W., & Liu, C. (1999). Convection initiation by density currents: Role of convergence, shear, and dynamical organization. *Monthly Weather Review*, *127*(10), 2455–2464. https://doi.org/10.1175/1520-0493(1999)127<2455:CIBDCR>2.0.CO;2

Moseley, C., Hohenegger, C., Berg, P., & Haerter, J. O. (2016). Intensification of convective extremes driven by cloud–cloud interaction. *Nature Geoscience*, *9*, 748–752.

Nie, J., & Kuang, Z. (2012). Responses of shallow cumulus convection to large-scale temperature and moisture perturbations: A comparison of large-eddy simulations and a convective parameterization based on stochastically entraining parcels. *Journal of the Atmospheric Sciences*, *69*(6), 1936–1956. https://doi.org/10.1175/JAS-D-11-0279.1

Purdom, J. F. W. (1976). Some uses of high-resolution GOES imagery in the mesoscale forecasting of convection and its behavior. *Monthly Weather Review*, *104*(12), 1474–1483. https://doi.org/10.1175/1520-0493(1976)104<1474:SUOHRG>2.0.CO;2

Rio, C., Hourdin, F., Grandpeix, J.-Y., & Lafore, J.-P. (2009). Shifting the diurnal cycle of parameterized deep convection over land. *Geophysical Research Letters*, *36*, L07809. https://doi.org/10.1029/2008GL036779

Romps, D. M., & Jeevanjee, N. (2016). On the sizes and lifetimes of cold pools. *Quarterly Journal of the Royal Meteorological Society*, *142*(696), 1517–1527. https://doi.org/10.1002/qj.2754

Rotunno, R., Klemp, J. B., & Weisman, M. L. (1988). A theory for strong, long-lived squall lines. *Journal of the Atmospheric Sciences*, *45*(3), 463–485. https://doi.org/10.1175/1520-0469(1988)045<0463:ATFSLL>2.0.CO;2

Shin, J. O. (2001). Colliding gravity currents (Ph.D. thesis), University of Cambridge.

Siebesma, A. P., Bretherton, C. S., Brown, A., Chlond, A., Cuxart, J., Duynkerke, P. G., et al. (2003). A large eddy simulation intercomparison study of shallow cumulus convection. *Journal of the Atmospheric Sciences*, *60*(10), 1201–1219. https://doi.org/10.1175/1520-0469(2003)60<1201:ALESIS>2.0.CO;2

Simpson, J. E. (1997). Gravity currents in the environment and the laboratory. In J. E. Simpson (Ed.), *Journal of Fluid Mechanics* (Vol. 352, pp. 374–378). Cambridge University Press. https://doi.org/10.1017/S0022112097227527

Skamarock, W. C., Weisman, M. L., & Klemp, J. B. (1994). Three-dimensional evolution of simulated long-lived squall lines. *Journal of the Atmospheric Sciences*, *51*(17), 2563–2584. https://doi.org/10.1175/1520-0469(1994)051<2563:TDEOSL>2.0.CO;2

Tompkins, A. M. (2001). Organization of tropical convection in low vertical wind shears: The role of water vapor. *Journal of the Atmospheric Sciences*, *58*(6), 529–545. https://doi.org/10.1175/1520-0469(2001)058<0529:OOTCIL>2.0.CO;2

Torri, G., & Kuang, Z. (2016a). A Lagrangian study of precipitation-driven downdrafts. *Journal of the Atmospheric Sciences*, *73*, 839–854. https://doi.org/10.1175/JAS-D-15-0222.1

Torri, G., & Kuang, Z. (2016b). Rain evaporation and moist patches in tropical boundary layers. *Geophysical Research Letters*, *43*, 9895–9902. https://doi.org/10.1002/2016GL070893

Torri, G., Kuang, Z., & Tian, Y. (2015). Mechanisms for convection triggering by cold pools. *Geophysical Research Letters*, *42*, 1943–1950. https://doi.org/10.1002/2015GL063227

van der Wiel, K., Gille, S. T., Llewellyn Smith, S. G., Linden, P. F., & Cenedese, C. (2017). Characteristics of colliding sea breeze gravity current fronts: A laboratory study. *Quarterly Journal of the Royal Meteorological Society*, *143*(704), 1434–1441. https://doi.org/10.1002/qj.3015

Wakimoto, R. M. (1982). The life cycle of thunderstorm gust fronts as viewed with Doppler radar and rawinsonde data. *Monthly Weather Review*, *110*(8), 1060–1082. https://doi.org/10.1175/1520-0493(1982)110<1060:TLCOTG>2.0.CO;2

Weaver, J. F., & Nelson, S. P. (1982). Multiscale aspects of thunderstorm gust fronts and their effects on subsequent storm development. *Monthly Weather Review*, *110*(7), 707–718. https://doi.org/10.1175/1520-0493(1982)110<0707:MAOTGF>2.0.CO;2

Weisman, M. L., & Rotunno, R. (2004). "A theory for strong long-lived squall lines" revisited. *Journal of the Atmospheric Sciences*, *61*(4), 361–382. https://doi.org/10.1175/1520-0469(2004)061<0361:ATFSLS>2.0.CO;2

Wilson, J. W., & Schreiber, W. E. (1986). Initiation of convective storms at radar-observed boundary-layer convergence lines. *Monthly Weather Review*, *114*(12), 2516–2536. https://doi.org/10.1175/1520-0493(1986)114<2516:IOCSAR>2.0.CO;2

Zhong, Q., Hussain, F., & Fernando, H. J. S. (2018). Quantification of turbulent mixing in colliding gravity currents. *Journal of Fluid Mechanics*, *851*, 125–147. https://doi.org/10.1017/jfm.2018.488